JACS
JOURNAL OF THE AMERICAN CHEMICAL SOCIETY

Article

A General Descriptor #E Enables the Quantitative Development of Luminescent Materials based on Photoinduced Electron Transfer

Weijie Chi, Jie Chen, Wenjuan Liu, Chao Wang, Qingkai Qi, Qinglong Qiao, Tee Meng Tan, Kangming Xiong, Xiao Liu, Keegan Kang, Young-Tae Chang, Zhaochao Xu, and Xiaogang Liu

J. Am. Chem. Soc., **Just Accepted Manuscript** • DOI: 10.1021/jacs.0c01473 • Publication Date (Web): 17 Mar 2020

A General Descriptor Δ*E* Enables the Quantitative Development of Luminescent Materials based on Photoinduced Electron Transfer

Weijie Chi,[†,#] Jie Chen,[‡,#] Wenjuan Liu,[‡,#] Chao Wang,[†,‡] Qingkai Qi,[‡] Qinglong Qiao,[‡] Tee Meng Tan,[†] Kangming Xiong,[‡] Xiao Liu,[§] Keegan Kang,[†] Young-Tae Chang,[§,*] Zhaochao Xu,[‡,*] Xiaogang Liu[†,*]

[†] Fluorescence Research Group, Singapore University of Technology and Design, 8 Somapah Road 487372, Singapore.

[‡] CAS Key Laboratory of Separation Science for Analytical Chemistry, Dalian Institute of Chemical Physics, Chinese Academy of Sciences 457 Zhongshan Road, Dalian 116023, China

[§] Department of Chemistry, POSTECH & Center for Self-assembly and Complexity, IBS, Pohang 37673, Republic of Korea

ABSTRACT: Photo-induced electron transfer (PET) is one of the most important mechanism for developing fluorescent probes and biosensors. Quantitative prediction of the quantum yields of these probes and sensors is crucial to accelerate the rational development of novel PET-based functional materials. Herein, we developed a general descriptor (Δ*E*) for predicting the quantum yield of PET probes, with a threshold value of ~0.6 eV. When Δ*E* < ~0.6 eV, the quantum yield is low (mostly <2%) due to the substantial activation of PET in polar environments; when Δ*E* > ~0.6 eV, the quantum yield is high because of the inhibition of PET. This simple yet effective descriptor is applicable to a wide range of fluorophores, such as BODIPY, fluorescein, rhodamine, and Si-Rhodamine. This Δ*E* descriptor not only enables us to establish new applications for existing PET probes but also quantitatively design novel PET-based fluorophores for wash-free bioimaging and AIEgen development.

INTRODUCTION

Photoinduced electron transfer (PET)[1-2] has been frequently employed for constructing numerous fluorescent probes to detect various species that are of considerable biological importance.[3-10] Modulating PET formations induces significant changes in the quantum yields of these probes, thus affording a convenient route to monitor analytes or environmental changes with high sensitivity, vivid visibility, and good spatiotemporal resolution. Accordingly, the accurate prediction of quantum yields represents one of the key requirements in the rational development of novel PET probes. Nevertheless, few simple and effective methods exist to quantitatively predict quantum yields,[11-12] especially when chemists venture into new fluorophore structural spaces in search for novel PET probes with tailored selectivity and sensitivity. To expedite the molecular engineering of such probes and expand their utility, it is imperative to formulate a fast and reliable approach to predict the quantum yields of PET probes, based on a deep understanding of their structure-property relationships.

Molecular structures of PET probes typically employ the 'fluorophore–spacer–receptor' format, as summarized by de Silva and co-workers (Figure 1a).[13-14] In the PET ON state, the quantum yield of the fluorophore ($\Phi_{PET\text{-}ON}$) is extremely low, because the fast PET rate substantially quenches fluorescence. In the PET OFF state, the fluorophore emits bright fluorescence (high quantum yield; $\Phi_{PET\text{-}OFF}$) as the PET process is inhibited upon the binding of the analyte at the receptor site (Figure 1b). A low $\Phi_{PET\text{-}ON}$ value is critical to ensure a large turn-on or turn-off ratio (approximately $\Phi_{PET\text{-}OFF}/\Phi_{PET\text{-}ON}$), which quantifies the sensitivity of the PET probe. It is of note that the "spacer" in a PET probe could also be removed (Figure 1a), by directly linking the receptor to the fluorophore (i.e., via a single C-C bond), such as in a series of PET probes developed by Nagano and Urano groups.[15]

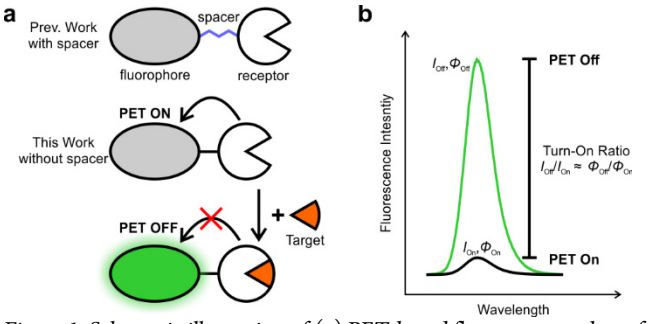

Figure 1. Schematic illustration of (a) PET-based fluorescent probes of the 'fluorophore-spacer-receptor' and 'fluorophore-receptor' formats; (b) the change of fluorescence intensity for a PET probe.

Significant efforts have been devoted to formulating equations for predicting the quantum yield of PET probes. The change in Gibbs free energy (Δ*G*), as described by the Rehm-Weller Equation proposed in 1968,[16] is an important descriptor to determine the quantum yields of PET probes (including both 'fluorophore–spacer–receptor' and 'fluorophore–receptor' formats), by assessing the thermodynamic feasibility of PET. In general, a negative Δ*G* suggests an inferior quantum yield due to the activation of PET. However, a more negative Δ*G* does not always suggest a lower quantum yield, i.e., due to the presence of the Marcus inverted region.[17-18] Moreover, the PET rate needs to kinetically compete with the fluorescence rate. Although the kinetics of PET could be quantified via Marcus equation in principle,[19-20] it is often

challenging to accurately quantify many parameters (such as electronic coupling matrix elements) of this equation.[21]

Importantly, for PET probes with the 'fluorophore–spacer–receptor' configuration, de Silva et al. firstly proposed that the relative energy levels of the frontier molecular orbitals (FMO) in a fluorophore and a receptor fragment can rationalize PET ON (low quantum yield) or OFF (high quantum yield) switching.[22] For example, d-PET is on only if the energy level of the highest occupied molecular orbital (HOMO) of the receptor fragment is higher than that of the fluorophore (Figure 2a); a-PET is feasible only if the lowest occupied molecular orbital (LUMO) of receptor is more stable than that of the fluorophore (Figure 2a), where the receptor functions as a fluorescence quencher. These ground-breaking works have generated profound implications for the rational design of PET probes.[5, 9, 13, 23-24] Nevertheless, it is worth highlighting that the MO representation indicates that the "apparent" change of electronic energy of FMO must be negative to turn on PET and quench fluorescence ($\Delta E < 0$). This indication, however, is not consistent with several experimental observations for PET probes with the 'fluorophore–receptor' format.[25]

Herein, by investigating ~140 *meso*-phenyl-substituted fluorescent dyes with the 'fluorophore–receptor' configuration, we discovered and rationalized a general descriptor (ΔE) for semi-quantitatively predicting the quantum yield of PET probes, with a counterintuitive threshold value of ~0.6 eV. Our data showed that when ΔE < ~0.6 eV, the quantum yields of the fluorophores were low (i.e., mostly <2%) in polar solvents, in contrast, when ΔE > ~0.6 eV, the quantum yields of the fluorophores were high in all medium (i.e., mostly >20%). We further demonstrated that the ΔE threshold of ~0.6 eV could accurately predict fluorescence quantum yields in a wide range of popular fluorophores, such as BODIPY, fluorescein, rhodamine, and Si-rhodamine dyes. The descriptor ΔE successfully enabled us to quantitatively design PET fluorescent probes for various bioimaging applications (such as wash-free bioimaging of lipid droplets and mitochondria), and accurately predict AIEgens. We believe that the descriptor ΔE will serve as a highly useful indicator for the efficient development of numerous PET-based luminescent materials.

RESULTS AND DISCUSSIONS

Correlation between ΔE and quantum yields of PET-based BODIPY dyes. Our initial investigations started with ***p*-NH₂-Ph-BDP** (**B4**; Figure S1), which quantum yield is very low in polar solvents (0.3% in methanol).[26] Previous reports suggested that a fast PET process quenched the fluorescence of such BODIPY dyes. Unfortunately, many of these studies did not include convincing experimental data to validate the PET process, such as observations of radical ions using time-resolved spectroscopic techniques. Moreover, to our surprise, our DFT/TD-DFT calculations show that **B4** does not possess any quenching orbitals sitting in between the HOMO and LUMO of the BODIPY fragment [Figures S1 and S2; See the "computational methods" section in the Supporting Information (SI)], suggesting the absence of both a-PET and d-PET according to the widely used MO representation of PET. These results clearly cannot explain the observed low quantum yields in **B4**. It is worth emphasizing again that a similar disagreement has also been noted in the fluorescein derivative.[25] These inconsistencies demand a thorough revision to the existing MO representation of the PET process.

The existing MO representation of PET involves the HOMOs and/or LUMOs of both the fluorophore and receptor moieties, where the latter serves as a quencher. The driving force for the PET process is energetically described as $\Delta E = E_{HOMO,\ fluorophore} - E_{HOMO,\ quencher}$ for a-PET (Figure 2a) and $\Delta E = E_{LUMO,\ quencher} - E_{LUMO,\ fluorophore}$ for d-PET (Figure 2a). When the fluorophore and quencher moieties are present in one molecule and computationally modeled together, the FMOs are typically HOMO-1, HOMO, LUMO, and LUMO+1 of this molecule. In such a case, the driving force for PET can be calculated by mapping these frontier molecular orbitals to either the fluorophore or the receptor moiety according to the electron density distribution, followed by calculating ΔE. The smaller value between $E_{HOMO,\ fluorophore} - E_{HOMO,\ quencher}$ and $E_{LUMO,\ quencher} - E_{LUMO,\ fluorophore}$ should be taken into consideration, to reflect the energetic preference of a-PET or d-PET. A negative ΔE is often deemed necessary for activating PET.

We collected the molecular structures and quantum yields of 83 *meso*-phenyl substituted BODIPY dyes from existing literature (Table S1), and calculated the energy levels of the FMOs of all these molecules using M062X/Def2SVP level of theory to derive ΔE (Figures S3 – S85). The results revealed an intriguing correlation between the quantum yields of these BODIPY dyes and their ΔE values: when ΔE > ~0.6 eV, the quantum yields of these fluorophores are high (i.e., Φ >10% for all such compounds, and Φ > 50% for 90% of these compounds); in contrast, when ΔE < ~0.6 eV, the quantum yields of these fluorophores in polar solvents are generally low (i.e., Φ < 10% for all such compounds and Φ < 2% for 80% of these compounds; Figures 2b and S86). It is worth emphasizing that these dyes employ rigid BODIPY fluorophores, which quantum yields are typically close to 1. That is, other fluorescence quenching mechanisms such as twisted intramolecular charge transfer (TICT) and formation of triplet excited states,[27-30] are mostly not applicable. Hence, the low quantum yields have been attributed to PET-induced fluorescence quenching. Our results suggested that ΔE of ~0.6 eV is a useful descriptor to predict the low/high quantum yields of PET-based fluorophores.

The threshold of ΔE = ~0.6 eV is apparently inconsistent with the existing MO representation of PET (which suggests ΔE = 0). In particular, the MO representation seems to indicate that PET in the region of 0 < ΔE < ~0.6 eV is energetically not feasible. However, many fluorophores with ΔE < ~0.6 eV demonstrated low quantum yields, suggesting that the "exception" in **B4** is not an anomaly. Employing a range-separated functional ωB97XD, we obtained similar computational results (Figure S87 and Table S2). It is important to note that this ΔE threshold is applicable only when a PET probe is the 'fluorophore-receptor' type and the quencher is close to the fluorophore (Figure S88).

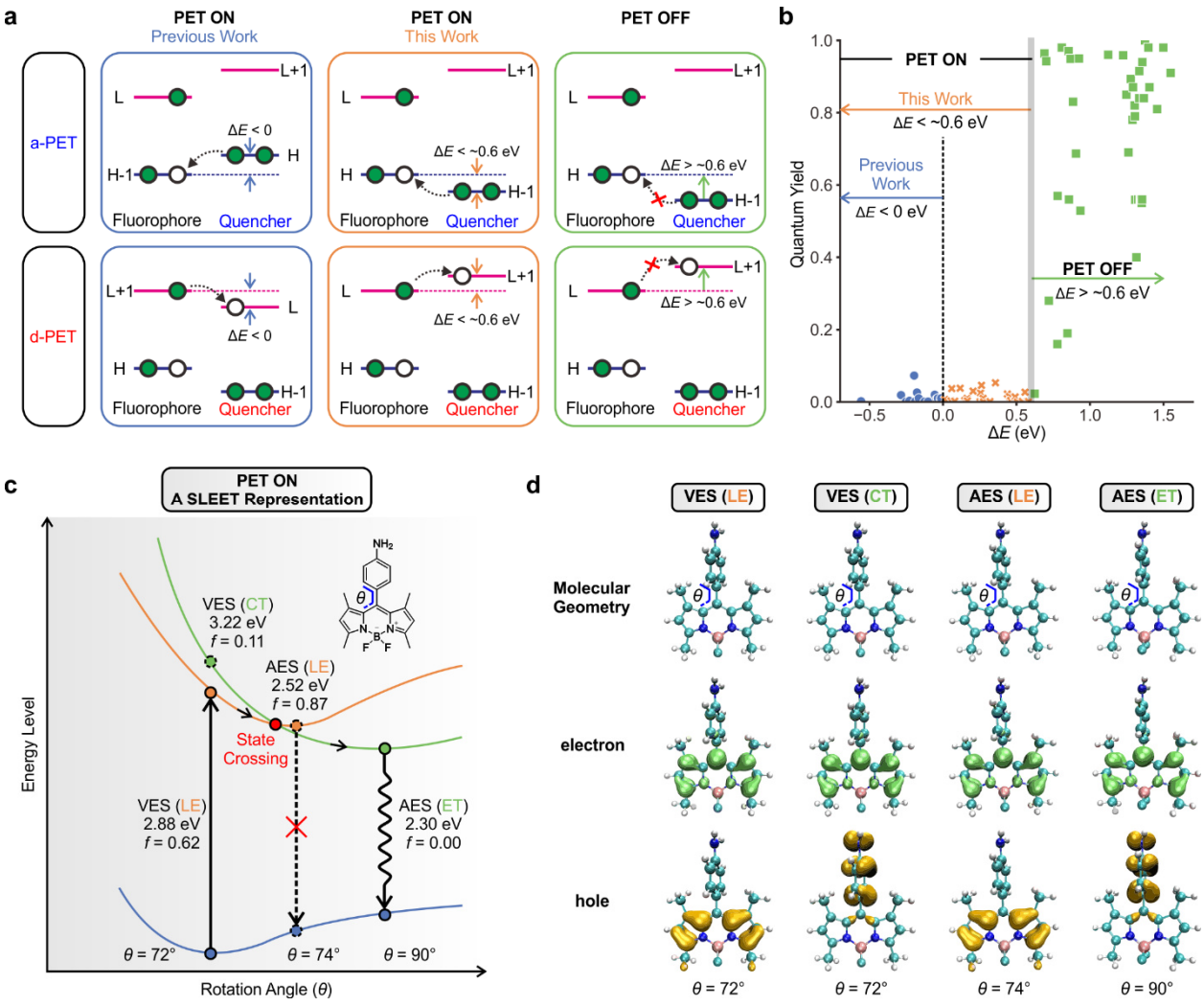

Figure 2. (a) Schematic illustration of the PET process upon the photoexcitation of a fluorophore, including both the donor-PET (d-PET) and acceptor-PET (a-PET). (b) Correlation between the experimental quantum yields and calculated ΔE (at the M062X/Def2SVP level of theory) of *meso*-phenyl BODIPY derivatives in polar solvents. (c) Schematic illustration of the State-crossing from a Locally-Excited to an Electron-Transfer state (SLEET) model, and calculated excitation/de-excitation energy (as well as oscillator strength *f*) of **B4** in methanol; the inset shows the molecular structure of **B4**; note that θ values are not drawn in scale for clarify. (d) Optimized molecular structures of **B4** in the ground and excited states, as well as the corresponding electron and hole distributions in methanol. VES and AES denoted vertically excited state and adiabatic excited state, respectively.

A SLEET model to rationalize the correlation between ΔE and quantum yields. To further understand the nature of the fluorescence quenching phenomenon in these BODIPY molecules, we performed detailed excited-state calculations of **B4** at M062X/TZVP level of theory in methanol. Our calculations show that the photoexcitation in **B4** resulted in a locally-excited (LE) state with a large oscillator strength (f = 0.62) in the Franck-Condon state (or the vertically excited state; Figure 2c), since both the photo-induced hole and electron are mainly located at the BODIPY scaffold (Figure 2d). However, upon geometry relaxation, a non-emissive electron-transfer (ET) state takes over the LE state and becomes the S_1 state in excited-state potential energy surfaces (PESs). The formation of this ET state is accompanied by the rotation of the *meso*-phenyl ring to a perpendicular alignment with respect to the BODIPY scaffold, which leads to a complete charge separation between the substituted *meso*-phenyl ring and the BODIPY scaffold and a negligible oscillator strength (f = 0) (Figures 2c and d). Accordingly, the PET formation and low quantum yield in **B4** can be rationalized by this State-crossing from a Locally-Excited to an Electron-Transfer state (SLEET) model.

A key difference between the popular MO representation of PET and the SLEET model concerns the treatment of the exciton binding energy in the excited states (especially in the ET state), which accounts for the difference between the "electronic" gap and the "optical" gap. The MO representation reflects the "electronic" gap, and the SLEET model considers the "optical" gap. The "optical" gap follows more closely with the photo-excitation and de-excitation processes. Consequently, the SLEET model is able to better explain experimental observations, including the "not feasible" PET region with $0 < \Delta E < \sim 0.6$ eV.

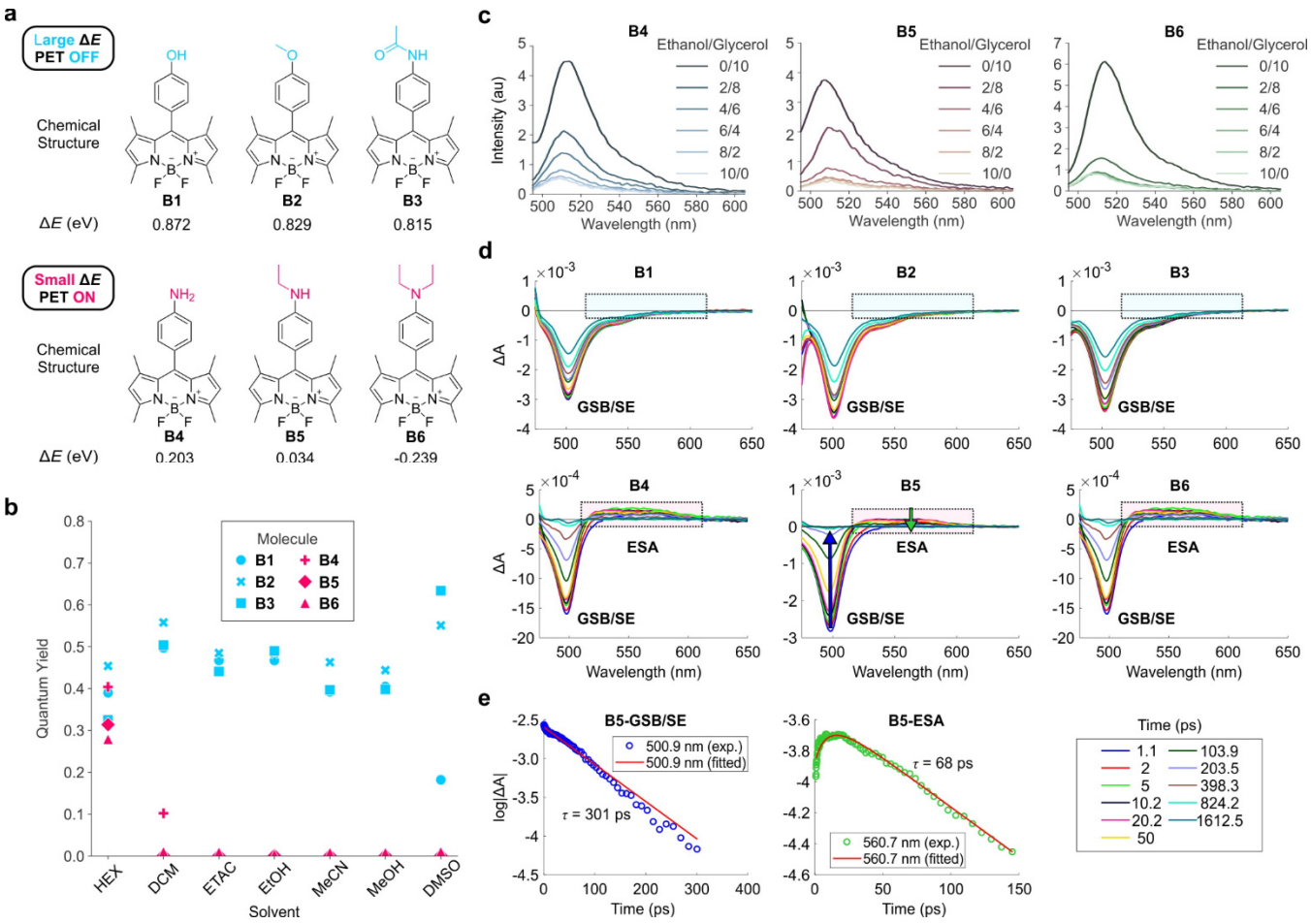

Figure 3. (a) Chemical structures and calculated Δ*E* values (in methanol) of **B1**—**B6**. (b) Experimental quantum yields of **B1**—**B6** in various solvents, including n-hexane (HEX), dichloromethane (DCM), ethyl acetate (ETAC), ethanol (EtOH), acetonitrile (MeCN), methanol (MeOH), and dimethyl sulfoxide (DMSO). (c) Viscosity responses of fluorescence intensities of **B4**—**B6**, in ethanol/glycerol mixtures with varied volume ratios. (d) Transient absorption spectra of **B1**—**B6** in ethanol, at different time delays. (e) Time evolutions, the best-fit functions, and the derived lifetime constants of the transient absorption signals at 500.9 nm and 560.7 nm for **B5** in ethanol.

Experimental validations of the PET mechanism. Next, we synthesized and characterized **B1**–**B6** (Figure 3a) in order to validate the PET mechanism (see the section of "Chemical synthesis of BODIPY derivatives" and Figures S89 – S94 of the SI). The UV—Vis absorption and fluorescence spectra, together with the fluorescence quantum yields of **B1**–**B6** were measured in various solvents with different polarities. The peak UV-Vis absorption wavelengths (496–502 nm) and emission wavelengths (506–514 nm) of **B1**–**B6** exhibited a slight shift (Figures S104 – S115) when the electron-donating groups at the phenyl ring were changed. The slight shift stemmed from a weak electronic coupling between the BODIPY scaffold and the *meso*-substituent groups (Table S3 and Figure S116). Importantly, the quantum yields of **B1**–**B3** (with $\Delta E >$ 0.6 eV) remain high in all tested solvents (Table S4 and Figure 3b). In contrast, **B4**–**B6** (with $\Delta E <$ 0.6 eV) are highly emissive only in low-polarity solvents (Φ = 0.404, 0.314, and 0.279 in hexane, respectively). They become almost nonfluorescent in polar solvents (Φ = 0.001, 0.001, and 0.004 in ethanol, respectively). According to the SLEET model, the polarity dependence of quantum yields is because the highly polar ET state becomes increasingly stable as solvent polarity increases (due to enhanced electrostatic interactions) and the state-crossing to the non-emissive ET state could be substantially activated only in high-polarity solvents.

Our calculations also showed that the state-crossing to the non-emissive ET state is accompanied by the rotation of the substituted *meso*-phenyl ring in BODIPYs. Accordingly, restricting such rotations (i.e., in high-viscosity solvents) should recover the fluorescence. Hence, we measured the viscosity dependence of the emission intensities in **B4**–**B6**. As we increased solvent viscosity by raising the volume ratio of glycerol in the ethanol/glycerol mixture, we noticed a considerable enhancement of fluorescence intensities in **B4**–**B6**, by 7—11 times (Figures 3c). These results are in good agreement with our theoretical calculations.

Radicals are usually short-lived but key species in PET processes.[24,31] We next performed transient absorption spectroscopy (TAS) measurements on **B4**–**B6** to establish the generation of radicals. TAS of **B1**-**B3** were collected as well for comparison. After photo-excitation, **B1**–**B3** only showed an overlapped ground-state bleaching (GSB) and stimulated emission (SE) band around 500 nm (Figure 3d), as the Stokes shifts of BODIPY dyes are small. These results indicated one dominant conformation in the excited state (i.e., the LE state). In stark contrast, in addition to this GSB/SE band, **B4**–**B6** exhibited one additional excited-state absorption (ESA) band at 530–600 nm (Figure 3d). Moreover, the decay lifetimes of the GSB/SE and the ESA are significantly different, i.e.,

301 ps for GSB/SE and 68 ps for ESA in **B5**, respectively (Figure 3e). These distinct spectra and lifetime suggest the presence of two excited-state conformations in **B4**–**B6**. Moreover, previous reports have shown that the transient absorption peaks of BODIPY radicals located at approximately 550 – 580 nm.[32-34] We thus attribute the observed ESA to the ET state of BODIPY dyes, as the ET state corresponds to the formation of radicals.

The solvent and viscosity dependence of the fluorescence intensity in **B4**–**B6**, as well as their transient absorption spectra, are entirely consistent with our calculations and provided unambiguous evidence on the occurrence of PET in these compounds. These observations also suggest that ΔE with a threshold value of ~0.6 eV could serve as a simple yet effective descriptor to predict substantial occurrences of PET in polar solvents and the resulted low quantum yields in PET probes.

Application of the descriptor ΔE. Both calculations and experiments have confirmed the reliability of descriptor ΔE in predicting low/high quantum yields (with a threshold value of ΔE = ~0.6 eV). We expect that ΔE will not only guide the quantitative design of PET-based fluorescence turn-on/off materials but also help to expand new applications for existing PET probes. As the polarity of the environment plays a significant role in controlling quantum yields of PET fluorescent probes,[35] we envisaged that PET-based luminescent materials could find a broad range of applications, such as fluorescence turn-on labeling of non-polar organelles, and the development of novel AIEgens (since molecular aggregation in polar solvents effectively reduces the local polarity of the AIEgens).[36-37]

Wash-free bioimaging of lipid droplets in live cells. Lipid droplets (LDs) are dynamic organelles that are involved in lipid storage and metabolism of cells. LDs play critical roles in many physiological processes,[38] and dysfunctions of LDs are related to many diseases, such as fatty liver, diabetes, obesity, cancer, and atherosclerosis.[39] Studying the dynamics of LD distributions in live cells are thus critical for gaining biological insights on these crucial cellular organelles.

We hypothesized that **B4**–**B6** could effectively stain LDs, due to preferential solvation in lipids than in aqueous solution. Moreover, because LDs provide a highly viscous (~50 cP; similar to the viscosity of the ethanol-glycerol mixture with a volume ratio of 43%:57%; Figure S117)[40] and non-polar environment, we would expect that **B4**–**B6** emit bright fluorescence in LDs due to the inhibition of PET. Besides, as the quantum yields of **B4**–**B6** are almost zero in high-polarity solvents, the background emissions from **B4**–**B6** in cytoplasm should be negligible even if a small amount of these compounds are present. These reasons encouraged us to perform wash-free bioimaging of LDs using **B4**–**B6**. As a comparison, we also stained cells using **B3**, whose quantum yields are high in all tested solvents. Consequently, relatively high background emissions from cytoplasm are expected.

Indeed, **B3** could penetrate cell membranes and stain live cells (Figure 4a). Colocalization experiments of this probe with **LD 540**, a commercially available LD imaging agent, demonstrates that **B3** emits bright fluorescence from lipid droplets (Figure 4a). However, this compound also generates noticeable emissions from the cytoplasm. The overall clarity of LDs is thus suboptimal. On the contrary, after staining live cells, PET probes **B4**–**B6** emit bright fluorescence only from lipid droplets (Figure 4b and Figure S118), which leads to a perfect overlap with emission signals of **LD 540**. The background emissions outsides of LDs are extremely low, although we did not perform any washing steps. The excellent wash-free LD bioimaging utilities of **B4**–**B6** further allows us to monitor the dynamics of LDs. For example, we noticed the merge of two small LDs into a big one at the time of 24 sec and 42 sec, respectively, with the assistance of **B4** (Figure 4c and Figure S119).

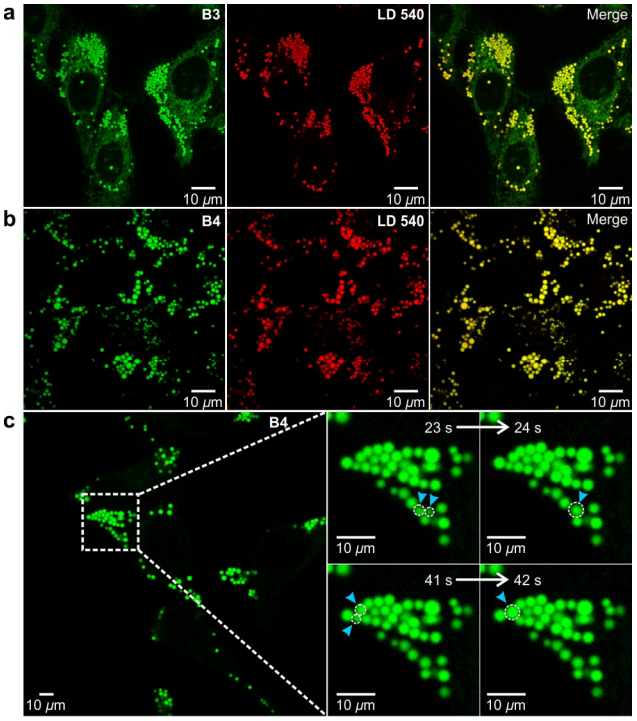

Figure 4. (a) Co-staining of HeLa cells using **B3** (1 μM) and **LD 540** (1 μM); green channel, **B3**; red channel, **LD 540**; yellow channel, the merged image. (b) Co-staining of HeLa cells using **B4** (1 μM) and **LD 540** (1 μM); green channel, **B4**; red channel, **LD 540**; yellow channel, the merged image. (c) Lipid droplet dynamics of HeLa cells, as revealed by **B4**. The merge of two small lipid droplets into a big one was observed at 24 sec and 42 sec, respectively.

Overall, guided by the descriptor ΔE, we demonstrate the excellent wash-free bioimaging utilities of PET-based probes in live-cell bioimaging, by utilizing the environmental dependence of PET.

Development of PET-based AIEgens. We next explored the applications of the PET mechanism in developing AIEgens. To date, luminescent materials with aggregation-induced emission (AIE) characteristics have found a broad range of applications, such as biosensors, photodynamic therapy agents, organic light-emitting diodes, and wave-guides.[36, 41-44] Formulating new mechanisms to design AIEgens is crucial to accelerate the development of functional AIE materials and applications.[37, 41, 45-46]

Based on the descriptor ΔE, we reason that **B5** and **B6** are potentially AIEgens: owing to the polarity dependence of PET, these probes are non-emissive in highly polar solvents. However, in parallel with molecular aggregation, the immediate local environment of these fluorophores becomes non-polar and large-amplitude intramolecular rotations are inhibited,[36] thus disabling the PET process and turning on emissions. Moreover, the *meso*-substitutes and the BODIPY scaffold of **B5** and **B6** are twisted with

respect to each other, endowing these compounds highly steric structures, which help to minimize π-π stacking in the aggregates or the solid-state. Finally, the alkyl-substitution to the amino group in **B5** and **B6** would further suppress potential intermolecular hydrogen bonding induced fluorescence quenching. These factors could collectively make **B5** and **B6** excellent AIEgens.

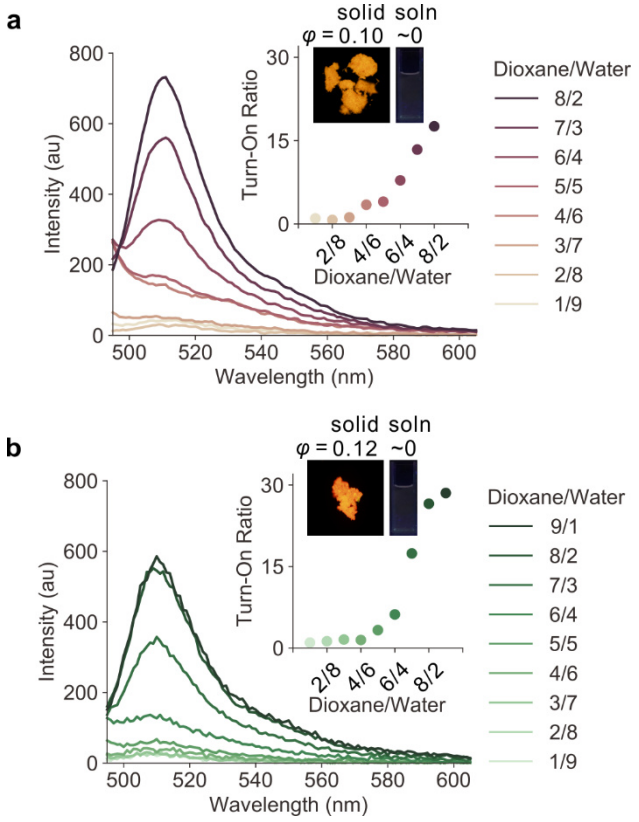

Figure 5. Fluorescence spectra of **B5** (a) and **B6** (b) in dioxane/water mixtures with different water fractions (f_w). The inset of (a) and (b) shows the changes of peak intensities of fluorescence spectra and the photographs of **B5** and **B6** in pure dioxane and powder state under UV irradiations, respectively.

We thus measured the UV-Vis absorption and emission spectra of **B5** and **B6** in ethanol/water (Figures S120 – S122) and dioxane/water mixtures (Figure 5). In pure dioxane or ethanol, **B5** and **B6** emitted almost no fluorescence. However, as the volume fraction (f_w) of water increases, the poor solubility of **B5** and **B6** in aqueous solution led to the formation of molecular aggregates. These aggregates greatly enhanced the emission intensities of **B5** and **B6** by up to 24 and 28 times, respectively. To further confirm the AIE characteristics of these compounds, we also measured the solid-state emissions of **B5** and **B6** powder. Indeed, bright solid-state luminescence with a quantum yield of 10% and 12 % was observed for **B5** and **B6**, respectively (Figure 5). The quantum yields in the solid powder are ~100 times as high as that in polar solvents.

Overall, as predicted by the descriptor ΔE, our results show that modulating PET formation serves as an effective mechanism for the rational development of AIEgens.

Generalization of the descriptor ΔE to other dye scaffolds. Motivated by the success of the descriptor ΔE in rationalizing and predicting quantum yields in BODIPY fluorophores, we then explored the possibility of applying descriptor ΔE to fluorescein, rhodamine and Si-rhodamine derivatives.[47-49] These dyes are the main-stream fluorophores and are heavily utilized in bioimaging, biosensing, and medical diagnostic applications.[50-51] Moreover, their *meso*-phenyl substituents have been modified to suit different applications based on the PET mechanism, similar to those of BODIPYs.

To our delight, our computational results showed that ΔE of ~0.6 eV could also serve as a useful threshold in evaluating the tendency of PET and semiquantitatively predicting the quantum yield of fluorescein, rhodamine and Si-rhodamine derivatives (Tables S5 and S6, Figures S123 – S179): ΔE < ~0.6 eV leads to a fast PET process and low quantum yields (Φ < 10% for all such compounds and Φ < 2% for 80% of these compounds); ΔE > ~0.6 eV significantly suppresses PET process and affords high quantum yields (i.e., Φ >10% for all but two such compounds, and Φ > 20% for 80% of these compounds) (Figures 6a and S180). These results show that the descriptor ΔE is generalizable to many chemical families when a quencher (receptor) is attached at a proximity to the fluorophore.

It is also interesting to note that in the PET OFF region, the quantum yields of those fluorophores are relatively lower than those of BODIPY-based fluorophores. This is because other mechanisms (such as TICT formations and hydrogen bond interactions) are still applicable in the fluorescence quenching of rhodamines,[27, 50] although PET is largely inhibited when ΔE > ~0.6 eV.

Quantitative designs of PET-based rhodamine dyes. To further verify the prediction power of the descriptor ΔE, we designed three new rhodamine dyes (**M1**, **M2**, and **M3** in Figure 6b). These compounds were locked in the "open-ring" structures, to avoid interference from spiro-cyclization reactions in conventional rhodamine dyes. Our quantum chemical calculations showed that ΔE in **M1** (1.024 eV) and **M2** (1.012 eV) were significantly larger than 0.6 eV, while ΔE in **M3** (0.522 eV) was less than 0.6 eV in methanol (Figures 6c, S181 – S183). Moreover, the HOMO and HOMO-1 of **M3** were located on the xanthene and *meso*-phenyl substituted groups, respectively (Figures 6d and S183). Hence, we predicted that the quantum yields of **M1** and **M2** should be high (>20%), and that of **M3** should be poor in polar solvents (as a result of substantial PET quenching).

Next, we synthesized and characterized **M1**, **M2**, and **M3** (see the section of "Chemical synthesis of rhodamine derivatives" and Figures S95 – S103 of the SI). The UV—Vis absorption (Figures S184 –S186) and fluorescence spectra (Figures S187 – S189), and the fluorescence quantum yields (Figure 6e; Table S7) of **M1**, **M2**, and **M3** were measured in various solvents with different polarities.

As expected, the quantum yields of **M1** and **M2** are high (30% and 26% in methanol, respectively). In contrast, the quantum yield of **M3** is only 1% in methanol.

These results show that the descriptor ΔE is highly effective in semi-quantitatively predicting the PET tendency and the resulting quantum yields in PET-based fluorophores. It is also worth mentioning that obtaining ΔE only requires ground-state calculations and are highly computationally efficient. ΔE is thus very useful for the quantitative design of PET-based luminescent materials, especially in large-scale computational screening.

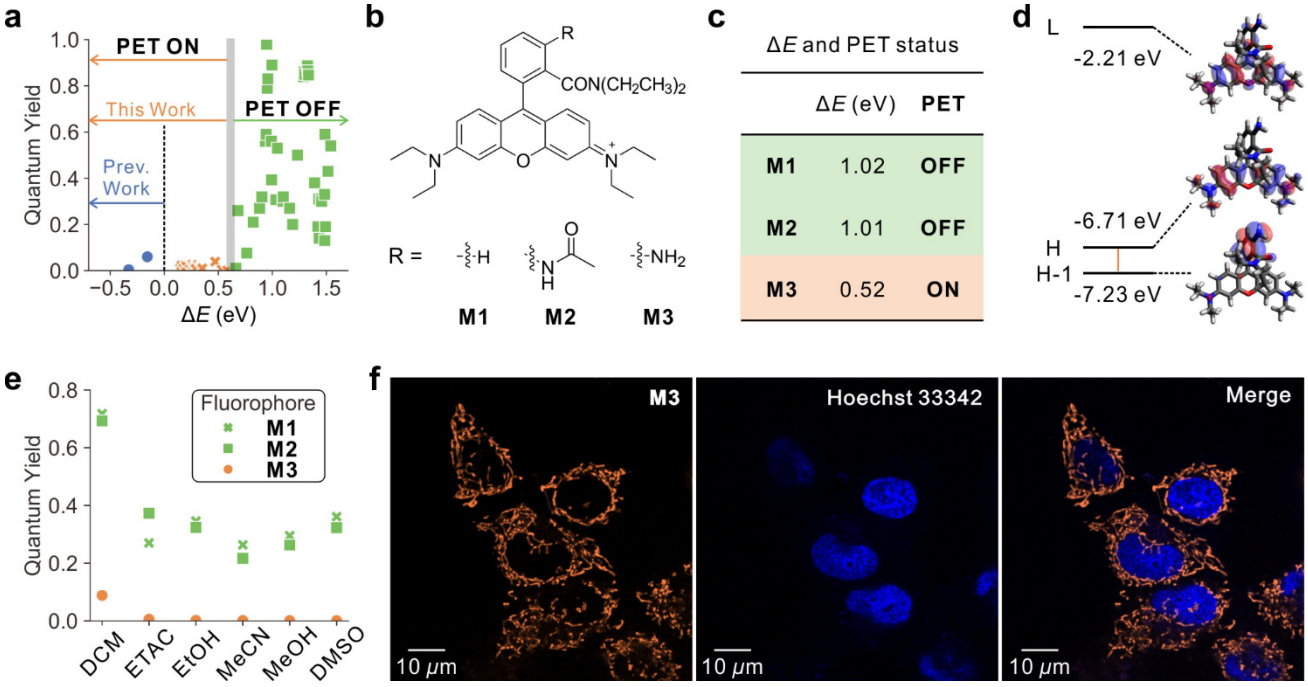

Figure 6. (a) Correlation between the experimental quantum yields and calculated ΔE (at the M062X/Def2SVP level of theory) of *meso*-phenyl rhodamine, Si-rhodamine and fluorescein derivatives in polar solvents, (b) designing three new rhodamine dyes (**M1** – **M3**), (c) the calculated ΔE of **M1** – **M3**, and prediction of PET status in ethanol, (d) calculated distributions and energies of FMO for **M3** in ethanol, (e) quantum yields of **M1**, **M2**, and **M3** in various solvents DCM, ETAC, EtOH, MeCN, MeOH, and DMSO, (f) co-stained live HeLa cells using **M3** (3 μM; orange channel) and Hoechst 33342 (a nucleus stain; 3 μM; blue channel) and the merged image.

Wash-free bioimaging of mitochondria using PET-based rhodamine dyes. Finally, we explored the wash-free bioimaging utilities of PET-based compound **M3**. This compound is weakly emissive in aqueous solution but highly emissive in DCM (due to the activation and disablement of PET, respectively). We expected that this compound remained dark in the cytoplasm. However, given that **M3** carries a positive charge, we foresaw that this compound could anchor onto mitochondria, which has a negative membrane potential.[52-53] Besides, since the membrane of mitochondria is non-polar, bright emissions from **M3** may be restored in mitochondria, thus realizing wash-free bioimaging.

We thus co-stained live HeLa cells using **M3** (3 μM) and Hoechst 33342 (a nucleus stain; 3 μM). Notably, **M3** successfully penetrated the cellular membrane and accumulated in mitochondria (Figure 6f). The localization of **M3** in mitochondria was subsequently validated via co-staining with **Cy5** (Figure S190). Compound **M3** and Hoechst 33342 collectively enabled the multi-color bioimaging of mitochondria and nucleus in a wash-free manner. We also tested the bioimaging performance of **M1** and **M2** for comparison. Unfortunately, **M2** exhibits poor cell permeability. While **M1** successfully entered cells and stained mitochondria (Figure S191), it also led to substantial background emissions and poor bioimaging quality. Overall, these results demonstrate the excellent wash-free bioimaging utilities of PET probes.

CONCLUSIONS

In summary, we discovered and rationalized a general descriptor ΔE to semi-quantitatively predict quantum yields of BODIPY, fluorescein, O/Si-rhodamines with the 'fluorophore-receptor' format. The value of ΔE can be obtained via a simple ground-state calculation in a highly efficient manner. When ΔE < ~0.6 eV, PET is "ON" and the quantum yield of the fluorophores in polar solvents is low (i.e., mostly <2%). In contrast, when ΔE > ~0.6 eV, PET is "OFF" and the quantum yield of the fluorophore is high (i.e., mostly >20%). As a proof of concept, we accurately predicted and rationally developed wash-free fluorescent stains of lipid droplets and mitochondria, as well as AIEgens, by modulating PET formations. We expect that the descriptor ΔE would serve as a simple and effective indicator for guiding the development of abundant PET-based luminescent materials.

ASSOCIATED CONTENT

Supporting Information

The Supporting Information is available free of charge on the ACS Publications website.

AUTHOR INFORMATION

Corresponding Author

* E-mail: xiaogang_liu@sutd.edu.sg
* E-mail: zcxu@dicp.ac.cn
* E-mail: ytchang@postech.ac.kr

Author Contributions

# These authors contributed equally.

Notes

The authors declare no competing financial interest.

ACKNOWLEDGMENT

This work is supported by Singapore University of Technology and Design (SUTD) and the SUTD-MIT International Design Centre (IDC) [T1SRCI17126, IDG31800104], National Natural Science

Foundation of China (21878286, 21908216), Dalian Institute of Chemical Physics (DMTO201603, TMSR201601) and Institute for Basic Science (IBS, Korea) [IBS-R077-A1]. The authors would like to acknowledge the use of the computing service of SUTD-MIT IDC and National Super-computing Center (Singapore).

REFERENCES

1. Dadashi-Silab, S.; Doran, S.; Yagci, Y. Photoinduced Electron Transfer Reactions for Macromolecular Syntheses. *Chem. Rev.* **2016,** *116*, 10212-10275.

2. Griesbeck, A. G.; Hoffmann, N.; Warzecha, K.-D. Photoinduced-Electron-Transfer Chemistry: From Studies on PET Processes to Applications in Natural Product Synthesis. *Acc. Chem. Res.* **2007,** *40*, 128-140.

3. Abo, M.; Urano, Y.; Hanaoka, K.; Terai, T.; Komatsu, T.; Nagano, T. Development of a Highly Sensitive Fluorescence Probe for Hydrogen Peroxide. *J. Am. Chem. Soc.* **2011,** *133*, 10629-10637.

4. Fujikawa, Y.; Urano, Y.; Komatsu, T.; Hanaoka, K.; Kojima, H.; Terai, T.; Inoue, H.; Nagano, T. Design and Synthesis of Highly Sensitive Fluorogenic Substrates for Glutathione S-Transferase and Application for Activity Imaging in Living Cells. *J. Am. Chem. Soc.* **2008,** *130*, 14533-14543.

5. Urano, Y.; Kamiya, M.; Kanda, K.; Ueno, T.; Hirose, K.; Nagano, T. Evolution of Fluorescein as a Platform for Finely Tunable Fluorescence Probes. *J. Am. Chem. Soc.* **2005,** *127*, 4888-4894.

6. Kawatani, M.; Yamamoto, K.; Yamada, D.; Kamiya, M.; Miyakawa, J.; Miyama, Y.; Kojima, R.; Morikawa, T.; Kume, H.; Urano, Y. Fluorescence Detection of Prostate Cancer by an Activatable Fluorescence Probe for PSMA Carboxypeptidase Activity. *J. Am. Chem. Soc.* **2019,** *141*, 10409-10416.

7. Ungati, H.; Govindaraj, V.; Narayanan, M.; Mugesh, G. Probing the Formation of a Seleninic Acid in Living Cells by the Fluorescence Switching of a Glutathione Peroxidase Mimetic. *Angew. Chem. Int. Ed.* **2019,** *58*, 8156-8160.

8. Goldberg, J. M.; Batjargal, S.; Chen, B. S.; Petersson, E. J. Thioamide Quenching of Fluorescent Probes through Photoinduced Electron Transfer: Mechanistic Studies and Applications. *J. Am. Chem. Soc.* **2013,** *135*, 18651-18658.

9. Gabe, Y.; Urano, Y.; Kikuchi, K.; Kojima, H.; Nagano, T. Highly Sensitive Fluorescence Probes for Nitric Oxide Based on Boron Dipyrromethene Chromophore Rational Design of Potentially Useful Bioimaging Fluorescence Probe. *J. Am. Chem. Soc.* **2004,** *126*, 3357-3367.

10. Filatov, M. A. Heavy-Atom-Free BODIPY Photosensitizers with Intersystem Crossing Mediated by Intramolecular Photoinduced Electron Transfer. *Org. Biomol. Chem.* **2020,** *18*, 10-27.

11. Peng, Q.; Shi, Q.; Niu, Y.; Yi, Y.; Sun, S.; Li, W.; Shuai, Z. Understanding the Efficiency Drooping of the Deep Blue Organometallic Phosphors: a Computational Study of Radiative and Non-radiative Decay Rates for Triplets. *J. Mater. Chem. C* **2016,** *4*, 6829-6838.

12. Niu, Y.; Li, W.; Peng, Q.; Geng, H.; Yi, Y.; Wang, L.; Nan, G.; Wang, D.; Shuai, Z. MOlecular MAterials Property Prediction Package (MOMAP) 1.0: a Software Package for Predicting the Luminescent Properties and Mobility of Organic Functional Materials. *Mol. Phys.* **2018,** *116*, 1078-1090.

13. Daly, B.; Ling, J.; de Silva, A. P. Current Developments in Fluorescent PET (Photoinduced Electron Transfer) Sensors and Switches. *Chem. Soc. Rev.* **2015,** *44*, 4203-4211.

14. de Silva, A. P. Luminescent Photoinduced Electron Transfer (PET) Molecules for Sensing and Logic Operations. *J. Phys. Chem. Lett.* **2011,** *2*, 2865-2871.

15. Kobayashi, H.; Ogawa, M.; Alford, R.; Choyke, P. L.; Urano, Y. New Strategies for Fluorescent Probe Design in Medical Diagnostic Imaging. *Chem. Rev.* **2010,** *110*, 2620-2640.

16. Weller, A. Electron-Transfer and Complex Formation in the Excited State. *Pure Appl. Chem.* **1968**, *16*, 115.

17. Goldsmith, Z. K.; Soudackov, Alexander. V.; Hammes-Schiffer, S. Theoretical Analysis of the Inverted Region in Photoinduced Proton-Coupled Electron Transfer. *Faraday Discuss.* **2019,** *216*, 363-378.

18. Parada, G. A.; Goldsmith, Z. K.; Kolmar, S.; Pettersson Rimgard, B.; Mercado, B. Q.; Hammarström, L.; Hammes-Schiffer, S.; Mayer, J. M. Concerted Proton-Electron Transfer Reactions in the Marcus Inverted Region. *Science* **2019,** *364*, 471-475.

19. Marcus, R. A. On the Theory of Oxidation-Reduction Reactions Involving Electron Transfer. I. *J. Chem. Phys.* **1956,** *24*, 966-978.

20. Marcus, R. A. Electron Transfer Reactions in Chemistry: Theory and Experiment (Nobel Lecture). *Angew. Chem. Int. Ed.* **1993,** *32*, 1111-1121.

21. Hsu, C.-P. The Electronic Couplings in Electron Transfer and Excitation Energy Transfer. *Acc. Chem. Res.* **2009,** *42*, 509-518.

22. de Silva, A. P.; Moody, T. S.; Wright, G. D. Fluorescent PET (Photoinduced Electron Transfer) Sensors as Potent Analytical Tools. *Analyst* **2009,** *134*, 2385-2393.

23. Zang, L.; Liu, R.; Holman, M. W.; Nguyen, K. T.; Adams, D. M. A Single-Molecule Probe Based on Intramolecular Electron Transfer. *J. Am. Chem. Soc.* **2002,** *124*, 10640-10641.

24. Miura, T.; Urano, Y.; Tanaka, K.; Nagano, T.; Ohkubo, K.; Fukuzumi, S. Rational Design Principle for Modulating Fluorescence Properties of Fluorescein-Based Probes by Photoinduced Electron Transfer. *J. Am. Chem. Soc.* **2003,** *125*, 8666-8671.

25. Zhou, P.; Liu, J.; Yang, S.; Chen, J.; Han, K.; He, G. The Invalidity of the Photo-Induced Electron Transfer Mechanism for Fluorescein Derivatives. *Phys. Chem. Chem. Phys.* **2012,** *14*, 15191-15198.

26. Pan, Z.-H.; Luo, G.-G.; Zhou, J.-W.; Xia, J.-X.; Fang, K.; Wu, R.-B. A Simple BODIPY-Aniline-Based Fluorescent Chemosensor as Multiple Logic Operations for the Detection of pH and CO_2 Gas. *Dalton Trans.* **2014,** *43*, 8499-8507.

27. Wang, C.; Qiao, Q.; Chi, W.; Chen, J.; Liu, W.; Tan, D.; McKechnie, S.; Lyu, D.; Jiang, X.-F.; Zhou, W.; Xu, N.; Zhang, Q.; Xu, Z.; Liu, X. Quantitative Design of Bright Fluorophores and AIEgens via the Accurate Prediction of Twisted Intramolecular Charge Transfer (TICT). *Angew. Chem. Int. Ed.* **2020**, DOI: 10.1002/anie.201916357.

28. Filatov, M. A.; Karuthedath, S.; Polestshuk, P. M.; Savoie, H.; Flanagan, K. J.; Sy, C.; Sitte, E.; Telitchko, M.; Laquai, F.; Boyle, R. W.; Senge, M. O. Generation of Triplet Excited States via Photoinduced Electron Transfer in *Meso*-Anthra-BODIPY: Fluorogenic Response toward Singlet Oxygen in Solution and in Vitro. *J. Am. Chem. Soc.* **2017,** *139*, 6282-6285.

29. Zheng, Q.; Jockusch, S.; Zhou, Z.; Altman, R. B.; Warren, J. D.; Turro, N. J.; Blanchard, S. C. On the Mechanisms of Cyanine Fluorophore Photostabilization. *J. Phys. Chem. Lett.* **2012,** *3*, 2200-2203.

30. Altman, R. B.; Terry, D. S.; Zhou, Z.; Zheng, Q.; Geggier, P.; Kolster, R. A.; Zhao, Y.; Javitch, J. A.; Warren, J. D.; Blanchard, S. C. Cyanine Fluorophore Derivatives with Enhanced Photostability. *Nat. Methods* **2012,** *9*, 68-71.

31. Swedin, R. K.; Zatsikha, Y. V.; Healy, A. T.; Didukh, N. O.; Blesener, T. S.; Fathi-Rasekh, M.; Wang, T.; King, A. J.; Nemykin, V. N.; Blank, D. A. Rapid Excited-State Deactivation of BODIPY Derivatives by a Boron-Bound Catechol. *J. Phys. Chem. Lett.* **2019,** *10*, 1828-1832.

32. Chi, W.; Qiao, Q.; Lee, R.; Liu, W.; Teo, Y. S.; Gu, D.; Lang, M. J.; Chang, Y.-T.; Xu, Z.; Liu, X. A Photoexcitation-Induced Twisted Intramolecular Charge Shuttle. *Angew. Chem. Int. Ed.* **2019,** *58*, 7073-7077.

33. Buck, J. T.; Boudreau, A. M.; DeCarmine, A.; Wilson, R. W.; Hampsey, J.; Mani, T. Spin-Allowed Transitions Control the Formation of Triplet Excited States in Orthogonal Donor-Acceptor Dyads. *Chem* **2019,** *5*, 138-155.

34. Benniston, A. C.; Clift, S.; Hagon, J.; Lemmetyinen, H.; Tkachenko, N. V.; Clegg, W.; Harrington, R. W. Effect on Charge Transfer and Charge Recombination by Insertion of a Naphthalene-Based Bridge in Molecular Dyads Based on Borondipyrromethene (BODIPY). *ChemPhysChem* **2012,** *13*, 3672-3681.

35. Sunahara, H.; Urano, Y.; Kojima, H.; Nagano, T. Design and Synthesis of a Library of BODIPY-Based Environmental Polarity Sensors Utilizing Photoinduced Electron-Transfer-Controlled Fluorescence ON/OFF Switching. *J. Am. Chem. Soc.* **2007,** *129*, 5597-5604.

36. Mei, J.; Leung, N. L. C.; Kwok, R. T. K.; Lam, J. W. Y.; Tang, B. Z. Aggregation-Induced Emission: Together We Shine, United We Soar! *Chem. Rev.* **2015,** *115*, 11718-11940.

37. Qi, Q.; Huang, L.; Yang, R.; Li, J.; Qiao, Q.; Xu, B.; Tian, W.; Liu, X.; Xu, Z. Rhodamine-Naphthalimide Demonstrated a Distinct Aggregation-Induced Emission Mechanism: Elimination of Dark-States via Dimer Interactions (EDDI). *Chem. Commun.* **2019,** *55*, 1446-1449.

38. Welte, M. A. Expanding Roles for Lipid Droplets. *Curr. Biol.* **2015,** *25*, R470-R481.

39. Gluchowski, N. L.; Becuwe, M.; Walther, T. C.; Farese Jr, R. V. Lipid Droplets and Liver Disease: From Basic Biology to Clinical Implications. *Nat. Rev. Gastro. Hepat.* **2017,** *14*, 343.

40. Song, C. W.; Tamima, U.; Reo, Y. J.; Dai, M.; Sarkar, S.; Ahn, K. H. A Rationally Designed Polarity–Viscosity Sensitive Probe for Imaging Lipid Droplets. *Dyes Pigments* **2019,** *171*, 107718.

41. Chen, Y.; Lam, J. W. Y.; Kwok, R. T. K.; Liu, B.; Tang, B. Z. Aggregation-Induced Emission: Fundamental Understanding and Future Developments. *Mater. Horizons* **2019,** *6*, 428-433.

42. Niu, G.; Zheng, X.; Zhao, Z.; Zhang, H.; Wang, J.; He, X.; Chen, Y.; Shi, X.; Ma, C.; Kwok, R. T. K.; Lam, J. W. Y.; Sung, H. H. Y.; Williams, I. D.; Wong, K. S.; Wang, P.; Tang, B. Z. Functionalized Acrylonitriles with Aggregation-Induced Emission: Structure Tuning by Simple Reaction-Condition Variation, Efficient Red Emission, and Two-Photon Bioimaging. *J. Am. Chem. Soc.* **2019,** *141*, 15111-15120.

43. Shi, Y.; Yin, G.; Yan, Z.; Sang, P.; Wang, M.; Brzozowski, R.; Eswara, P.; Wojtas, L.; Zheng, Y.; Li, X.; Cai, J. Helical Sulfono-γ-AApeptides with Aggregation-Induced Emission and Circularly Polarized Luminescence. *J. Am. Chem. Soc.* **2019,** *141*, 12697-12706.

44. Yang, H.; Liu, Y.; Guo, Z.; Lei, B.; Zhuang, J.; Zhang, X.; Liu, Z.; Hu, C. Hydrophobic Carbon Dots with Blue Dispersed Emission and Red Aggregation-Induced Emission. *Nat. Commun.* **2019,** *10*, 1789.

45. Tu, Y.; Liu, J.; Zhang, H.; Peng, Q.; Lam, J. W. Y.; Tang, B. Z. Restriction of Access to the Dark State: A New Mechanistic Model for Heteroatom-Containing AIE Systems. *Angew. Chem. Int. Ed.* **2019,** *58*, 14911-14914.

46. Kokado, K.; Sada, K. Consideration of Molecular Structure in the Excited State to Design New Luminogens with Aggregation-Induced Emission. *Angew. Chem. Int. Ed.* **2019,** *58*, 8632-8639.

47. Wang, L.; Du, W.; Hu, Z.; Uvdal, K.; Li, L.; Huang, W. Hybrid Rhodamine Fluorophores in the Visible/NIR Region for Biological Imaging. *Angew. Chem. Int. Ed.* **2019,** *58*, 14026-14043.

48. Yan, F.; Fan, K.; Bai, Z.; Zhang, R.; Zu, F.; Xu, J.; Li, X. Fluorescein Applications as Fluorescent Probes for the Detection of Analytes. *TrAC-TrendD. Anal. Chem.* **2017,** *97*, 15-35.

49. Deng, F.; Xu, Z. Heteroatom-Substituted Rhodamine Dyes: Structure and Spectroscopic Properties. *Chin. Chem. Lett.* **2019,** *30*, 1667-1681.

50. Ye, Z.; Yang, W.; Wang, C.; Zheng, Y.; Chi, W.; Liu, X.; Huang, Z.; Li, X.; Xiao, Y. Quaternary Piperazine-Substituted Rhodamines with Enhanced Brightness for Super-Resolution Imaging. *J. Am. Chem. Soc.* **2019,** *141*, 14491-14495.

51. Qi, Q.; Chi, W.; Li, Y.; Qiao, Q.; Chen, J.; Miao, L.; Zhang, Y.; Li, J.; Ji, W.; Xu, T.; Liu, X.; Yoon, J.; Xu, Z. A H-Bond Strategy to Develop Acid-Resistant Photoswitchable Rhodamine Spirolactams for Super-Resolution Single-Molecule Localization Microscopy. *Chem. Sci.* **2019,** *10*, 4914-4922.

52. Kathayat, R. S.; Cao, Y.; Elvira, P. D.; Sandoz, P. A.; Zaballa, M.-E.; Springer, M. Z.; Drake, L. E.; Macleod, K. F.; van der Goot, F. G.; Dickinson, B. C. Active and Dynamic Mitochondrial S-Depalmitoylation Revealed by Targeted Fluorescent Probes. *Nat. Commun.* **2018,** *9*, 334.

53. Long, L.; Huang, M.; Wang, N.; Wu, Y.; Wang, K.; Gong, A.; Zhang, Z.; Sessler, J. L. A Mitochondria-Specific Fluorescent Probe for Visualizing Endogenous Hydrogen Cyanide Fluctuations in Neurons. *J. Am. Chem. Soc.* **2018,** *140*, 1870-1875.

for TOC only

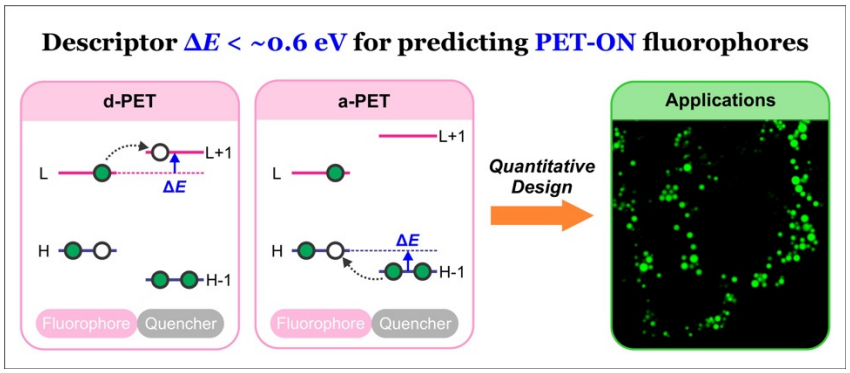
Descriptor ΔE < ~0.6 eV for predicting PET-ON fluorophores
d-PET
L+1
L
ΔE
H
H-1
Fluorophore
Quencher
a-PET
L+1
L
ΔE
H
H-1
Fluorophore
Quencher
Quantitative Design
Applications

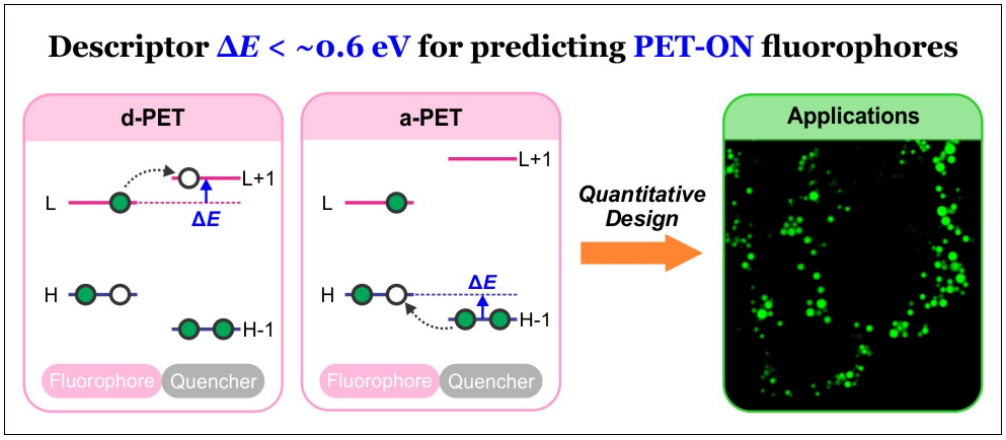
Descriptor ΔE < ~0.6 eV for predicting PET-ON fluorophores
d-PET
L+1
L
ΔE
H
H-1
Fluorophore
Quencher
a-PET
L+1
L
ΔE
H
H-1
Fluorophore
Quencher
Quantitative Design
Applications

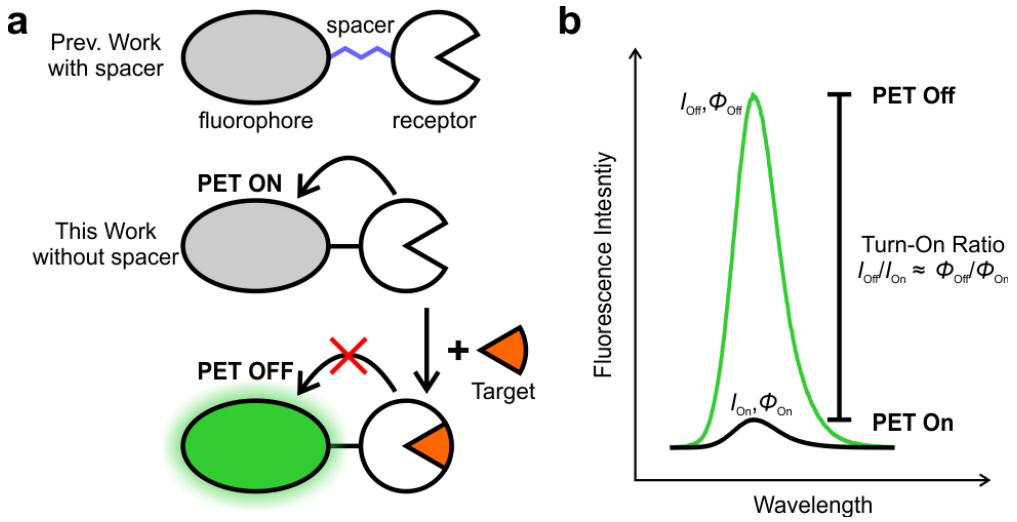

Figure 1. Schematic illustration of (a) PET-based fluorescent probes of the 'fluorophore-spacer-receptor' and 'fluorophore-receptor' formats; (b) the change of fluorescence intensity for a PET probe.

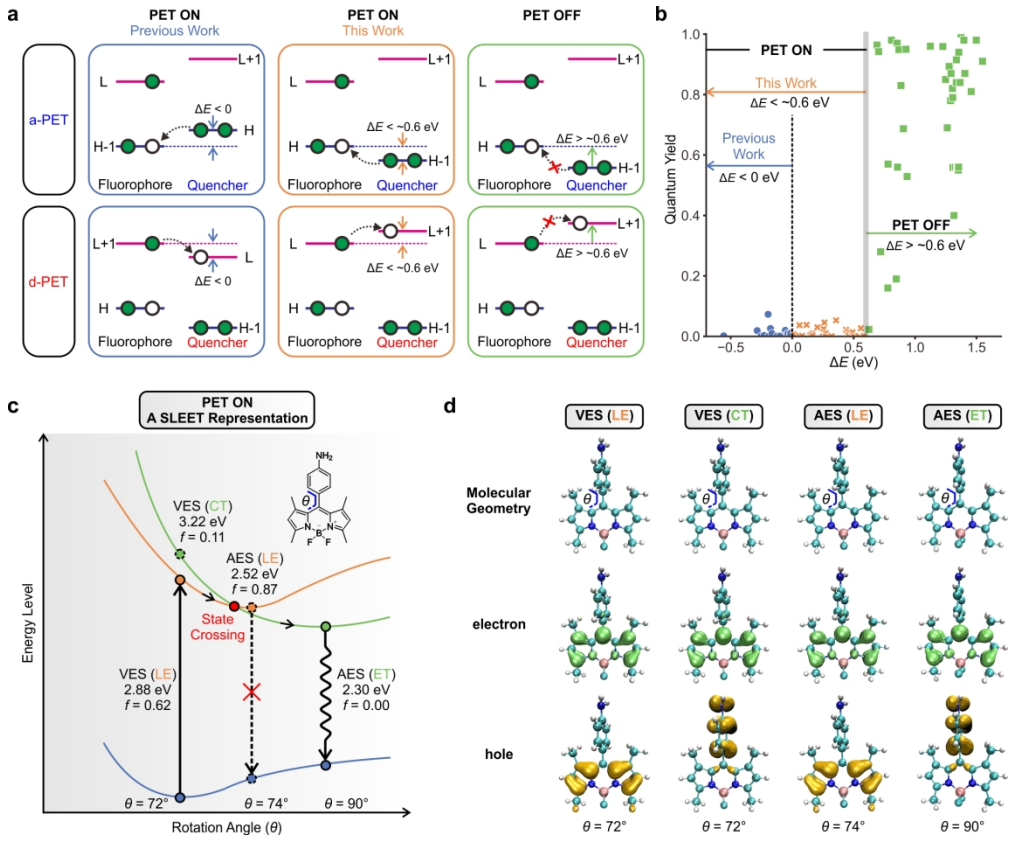

Figure 2. (a) Schematic illustration of the PET process upon the photoexcitation of a fluorophore, including both the donor-PET (d-PET) and acceptor-PET (a-PET). (b) Correlation between the experimental quantum yields and calculated ΔE (at the M062X/Def2SVP level of theory) of meso-phenyl BODIPY derivatives in polar solvents. (c) Schematic illustration of the State-crossing from a Locally-Excited to an Electron-Transfer state (SLEET) model, and calculated excitation/de-excitation energy (as well as oscillator strength f) of B4 in methanol; the inset shows the molecular structure of B4; note that θ values are not drawn in scale for clarify. (d) Optimized molecular structures of B4 in the ground and excited states, as well as the corresponding electron and hole distributions in methanol. VES and AES denoted vertically excited state and adiabatic excited state, respectively.

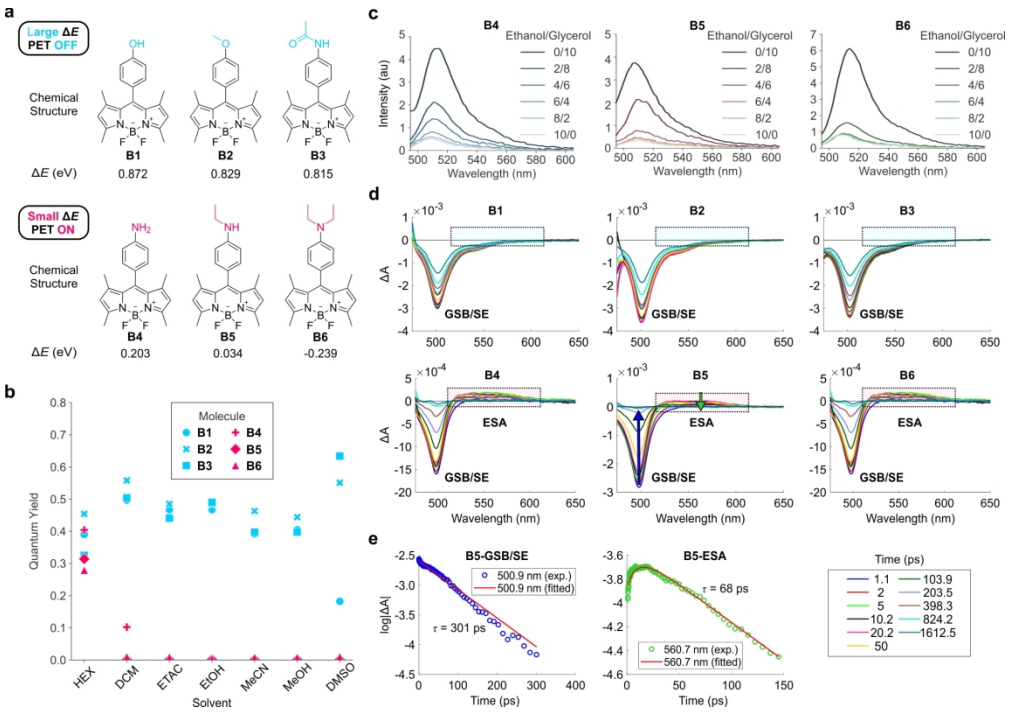

Figure 3. (a) Chemical structures and calculated ΔE values (in methanol) of B1—B6. (b) Experimental quantum yields of B1—B6 in various solvents, including n-hexane (HEX), dichloromethane (DCM), ethyl acetate (ETAC), ethanol (EtOH), acetonitrile (MeCN), methanol (MeOH), and dimethyl sulfoxide (DMSO). (c) Viscosity responses of fluorescence intensities of B4—B6, in ethanol/glycerol mixtures with varied volume ratios. (d) Transient absorption spectra of B1—B6 in ethanol, at different time delays. (e) Time evolutions, the best-fit functions, and the derived lifetime constants of the transient absorption signals at 500.9 nm and 560.7 nm for B5 in ethanol.

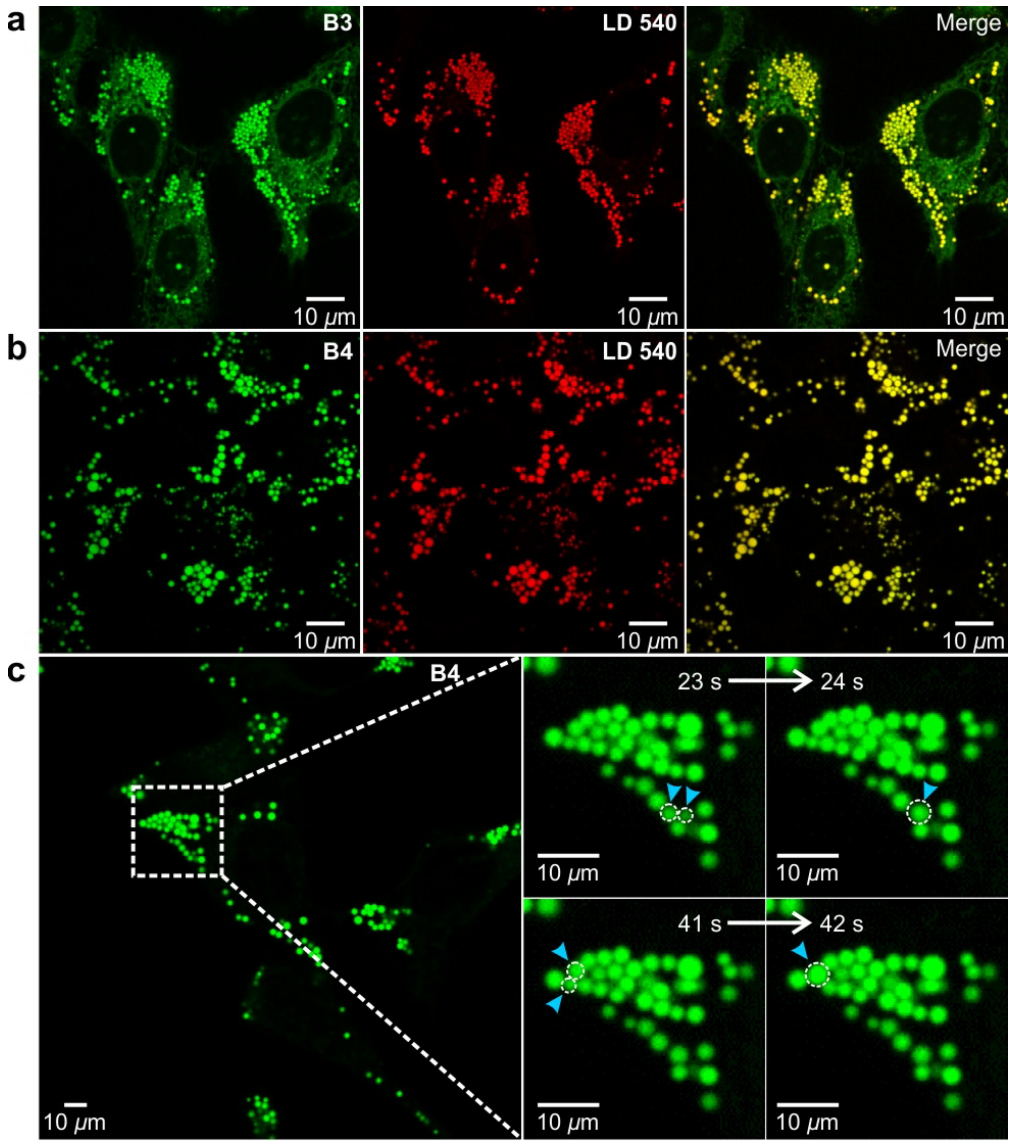

Figure 4. (a) Co-staining of HeLa cells using B3 (1 μM) and LD 540 (1 μM); green channel, B3; red channel, LD 540; yellow channel, the merged image. (b) Co-staining of HeLa cells using B4 (1 μM) and LD 540 (1 μM); green channel, B4; red channel, LD 540; yellow channel, the merged image. (c) Lipid droplet dynamics of HeLa cells, as revealed by B4. The merge of two small lipid droplets into a big one was observed at 24 sec and 42 sec, respectively.

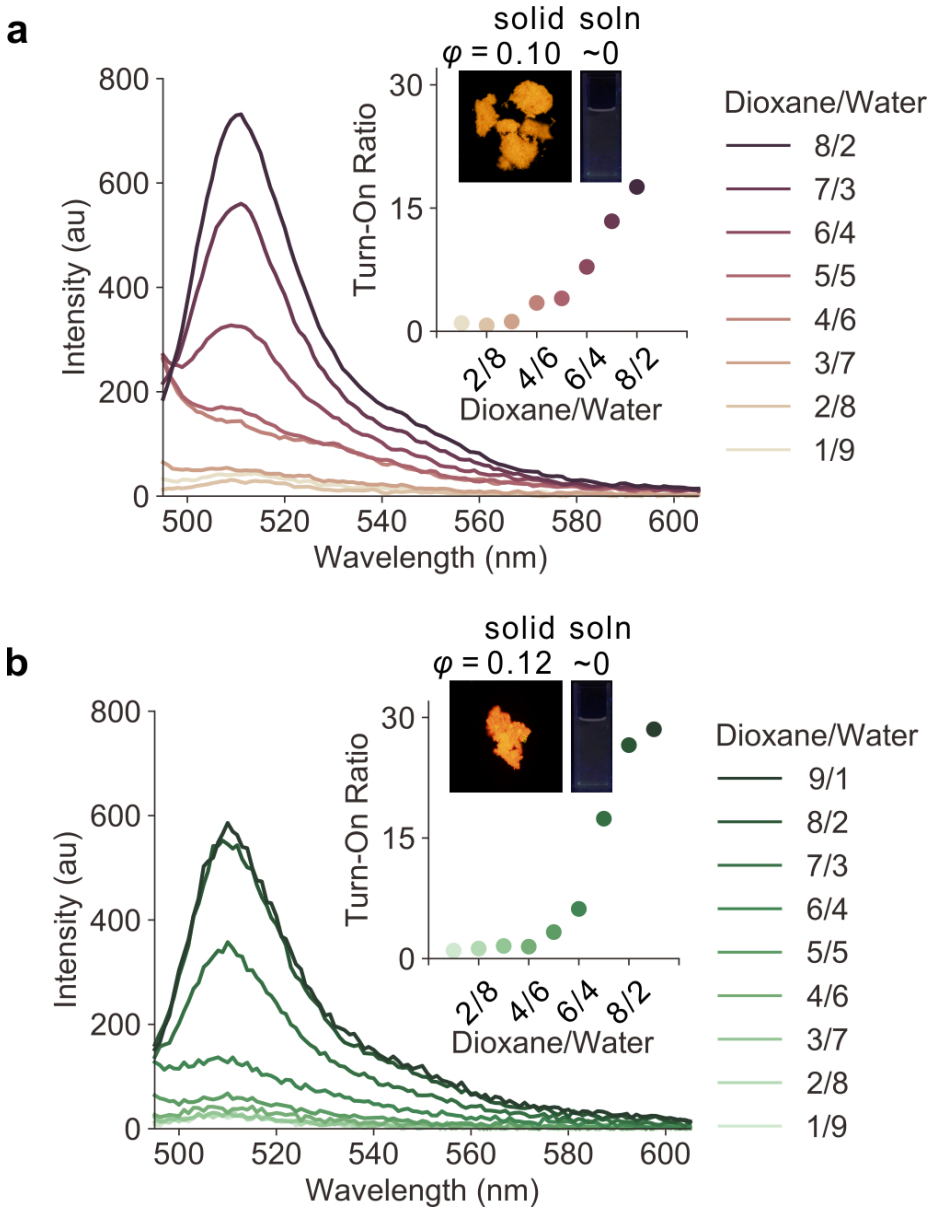

Figure 5. Fluorescence spectra of B5 (a) and B6 (b) in dioxane/water mixtures with different water fractions (fw). The inset of (a) and (b) shows the changes of peak intensities of fluorescence spectra and the photographs of B5 and B6 in pure dioxane and powder state under UV irradiations, respectively.

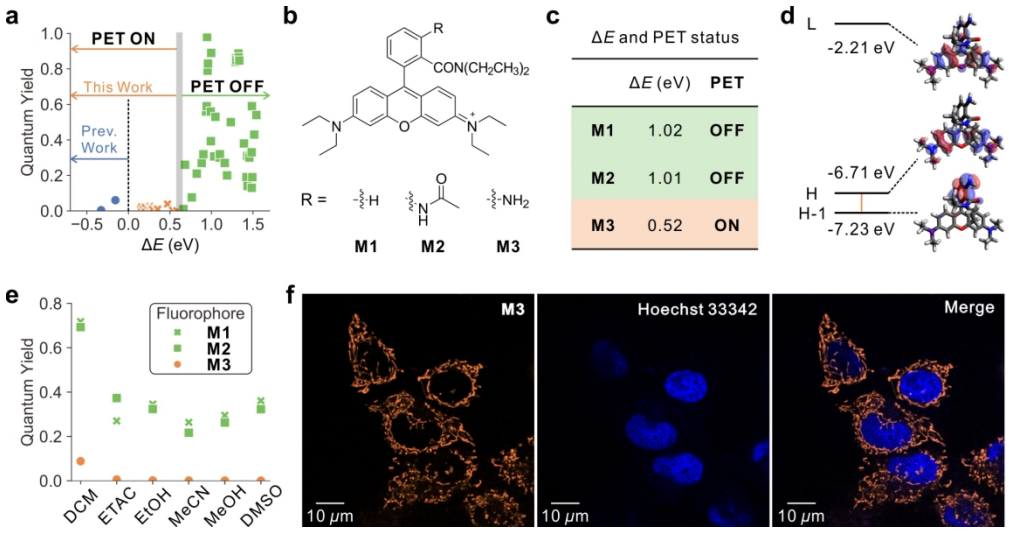

Figure 6. (a) Correlation between the experimental quantum yields and calculated ΔE (at the M062X/Def2SVP level of theory) of meso-phenyl rhodamine, Si-rhodamine and fluorescein derivatives in polar solvents, (b) designing three new rhodamine dyes (M1 – M3), (c) the calculated ΔE of M1 – M3, and prediction of PET status in ethanol, (d) calculated distributions and energies of FMO for M3 in ethanol, (e) quantum yields of M1, M2, and M3 in various solvents DCM, ETAC, EtOH, MeCN, MeOH, and DMSO, (f) co-stained live HeLa cells using M3 (3 μM; orange channel) and Hoechst 33342 (a nucleus stain; 3 μM; blue channel) and the merged image.